



# ENSO and PDO-related interannual and interdecadal variations in the wintertime sea surface temperature in a typical subtropical strait

Yimin Zhang<sup>1</sup> · Zhonghua Zhao<sup>1</sup> · Enhui Liao<sup>2</sup> · Yuwu Jiang<sup>1</sup>

Received: 11 October 2021 / Accepted: 19 March 2022 / Published online: 4 June 2022  
© The Author(s), under exclusive licence to Springer-Verlag GmbH Germany, part of Springer Nature 2022

## Abstract

The Taiwan Strait has the largest temporal variability in the wintertime sea surface temperature (SST) along the China coast. The warming and cooling trends reach about  $\pm 1$  °C per decade in winter during 1982–1999 and 1999–2014, respectively, which are about 4 times larger than neighboring coastal area and open ocean. Previous studies have noted these opposite trends, but the cause remains unclear due to insufficient study on teleconnections of this local signals to large-scale climate signals (e.g., Pacific Decadal Oscillation, PDO; El Niño–Southern Oscillation, ENSO). Using different period filters, wintertime SST anomaly in the Taiwan Strait (TS-SSTa) of different timescales were separated and connected to the large-scale climate signals. Besides the impact of global warming, we also found that the interdecadal signal of PDO contribute significantly to the warming and cooling trends of the wintertime TS-SSTa during 1982–2014 (mostly the positive PDO phase). During the positive PDO phase, a sea level pressure (SLP) dipole develops at the North Pacific, leading to a northeasterly wind jet along the Eurasian eastern coast, and affecting the interdecadal wintertime TS-SSTa through the East Asia Winter Monsoon (EAWM) and North Pacific Subtropical Gyre. During the negative PDO phase, the influence from North Pacific weakens, and the tropical Pacific has a greater influence on the interannual wintertime TS-SSTa through the northward movement of the ENSO-related cyclone/anticyclone anomaly over East Asia. Thus, the influence from North Pacific (PDO) and tropical Pacific (ENSO) alternately control the TS-SSTa variation during the positive and negative PDO phases.

**Keywords** Sea surface temperature · Pacific Decadal Oscillation · El Niño–Southern Oscillation · North Pacific Oscillation · North Pacific Gyre Oscillation · Taiwan Strait

## 1 Introduction

The East Asia Winter Monsoon (EAWM) is one of the most conspicuous climate phenomena that often brings severe cold surges and heavy snow to China during the boreal winter season (Ma and Chen 2021). It is associated with a powerful atmospheric circulation system and is generated by the significant thermal contrast between the large Eurasian landmass and the Indo–Pacific Ocean (Ding and Krishnamurti

1987). The EAWM has significant impacts on both local and remote climates (Chang and Lau 1982; Huang et al. 2007). Consequently, efforts were made to understand the EAWM variability and its governing processes (e.g., Huang et al. 2003; Huang et al. 2007; Wang et al. 2010). Previous studies reported that EAWM can be influenced by both the extratropical (Gong et al. 2001; Huang et al. 2017; Wu et al. 2006, 2009) and tropical climate variabilities (Annamalai et al. 2005; Ma and Chen 2021).

The El Niño–Southern Oscillation (ENSO) is recognized as a significant factor influencing the EAWM variability (Webster et al. 1998; Zhang et al. 1996). The ENSO is characterized with a strong interannual sea surface temperature (SST) variability over the tropical Pacific and is known to have strong impacts on the interannual variabilities of both the tropics and extra-tropics (Alexander et al. 2002; Ma and Chen 2021). Many studies focused on how the ENSO affects EAWM. Zhang et al. (1996) argued that

✉ Yuwu Jiang  
ywjiang@xmu.edu.cn

<sup>1</sup> State Key Laboratory of Marine Environmental Science, College of Ocean and Earth Sciences, Xiamen University, 361102 Xiamen, China

<sup>2</sup> Department of Geosciences, Princeton University, Princeton, NJ, USA

the El Niño can suppress convections over the western tropical Pacific. Wang et al. (2000); Zhang et al. (2017), and Kim et al. (2017) suggested that the ENSO impacts the EAWM primarily through the formation of an anomalous low-tropospheric anticyclonic/cyclonic circulation over the western North Pacific near the Philippines. They noted that an anomalous low-level anticyclone develops during the mature phase of El Niño in boreal winter and weakens the EAWM through a southwesterly wind anomaly in the western flank of the anticyclone. Consequently, the mature phase of El Niño is often accompanied by a weaker EAWM, lower surface heat loss from the ocean, incoming of warmer water from the south, and a correspondingly warmer SST in the China coastal seas. In contrast, the mature phase of La Niña is accompanied by a stronger EAWM and a colder SST in the China coastal seas (He and Wang 2013; Wang et al. 2000, 2008; Zhang et al. 1997).

Meanwhile, previous studies reported that the ENSO–EAWM relationship can be modulated by the North Pacific interdecadal climate variabilities such as the Pacific Decadal Oscillation (PDO, Kim et al. 2014; Wang et al. 2008). The PDO is the most dominant interdecadal SST oscillation in the North Pacific (Gershunov and Barnett 1998; Mantua et al. 1997; Wang et al. 2008, 2013) noted that the relationship between the ENSO and EAWM is not robust on the interannual timescale when the PDO is in its positive phase, though

ENSO has a strong impact on the EAWM when the PDO is in its negative phase. In addition, Kim et al. (2014) argued that the ENSO–EAWM relationship can be significantly strengthened when the PDO and ENSO are in phase, i.e., when El Niño occurs during the positive PDO phase or La Niña occurs during the negative PDO phase. In contrast, the EAWM remains relatively unchanged when the PDO and ENSO are out of phase.

The North Pacific Oscillation (NPO) is characterized by a large-scale atmospheric meridional dipole in the SLP and geopotential height over the North Pacific (Rogers 1981; Wallace and Gutzler 1981). The corresponding large-scale oceanic oscillation forced by the NPO is known as the North Pacific Gyre Oscillation (NPGO, Chhak et al. 2009; Di Lorenzo et al. 2008). As the second dominant EOF mode of winter sea surface height variability in the North Pacific, NPGO describes the strength variability of North Pacific Subtropical Gyre, a circulation system composed of Kuroshio, Kuroshio extension, North Pacific Current, California Current, and North Equatorial Current (Jiang et al. 2013; Joh and Di Lorenzo 2017) found a significant correlation between winter NPGO and the following winter PDO from extratropical/tropical teleconnections, implying the close relationship between the NPGO and PDO. Moreover, Di Lorenzo et al. (2010) found the NPGO is also closely related with ENSO, especially the central Pacific El Niño events.

The Taiwan Strait is located in the subtropical monsoon regime of the western North Pacific, and it links two marginal seas, namely, the East China Sea and the South China Sea (Fig. 1). The average depth of the Taiwan Strait is roughly 50 m. The detailed bathymetry is complicated and comprises a deep submarine channel in the southeast, a mid-strait ridge, and a submarine valley in the northern strait (Boggs et al. 1979). The circulation, which is determined by the currents and temperature and salinity distributions, thus shows a complex pattern that depends on the bathymetry and the East Asian monsoon wind (Jan et al. 2002, 2006; Yang 2007). In winter (approximately from mid-December to the following mid-March) when the northeasterly monsoon wind prevails, the western part of the strait is dominated by a southward-flowing coastal current known as the China Coastal Current (CCC, Hong et al. 2011; Zhao et al. 2020). It brings cold and less-saline water from the Yellow Sea and East China Sea through the strait into the South China Sea as far south as the Hainan Island (110°E, 20°N) in years of anomalously strong monsoon (Guan and Fang 2006; Hu et al. 2010; Pan et al. 2013). The eastern part of the strait is dominated by a northward-flowing current that flows against the monsoon wind and brings warm and more-saline water from the Kuroshio and South China Sea to the East China Sea (Chen et al. 2016; Jan et al. 2006; Jan et al. 2002). Yang (2007) suggested that the warm current is

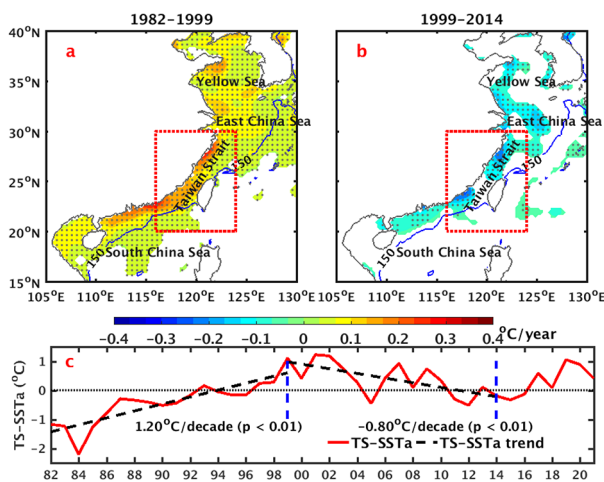


**Fig. 1** Sea surface temperature (SST) anomaly trend (from the OISST data, color shading, °C/year) in the China coastal seas during 1982–1999 (a) and 1999–2014 (b). Color shading and gray points represent the SST trends at the 90% and 95% significance levels, respectively. The solid blue line represents the 150 m isobath, presenting a steep slope. The dashed red box denotes the area of the Taiwan Strait. (c) The Taiwan Strait–SST anomaly (TS-SSTa) time series from 1982 to 2021, area-averaged within the dashed red box in (a) and (b) with water depth less than 150 m

driven by the northward pressure head of the Kuroshio. A cross-strait recirculation pattern often develops in the strait under the conflict between the wind and the pressure head, resulting in fronts where the cold and less-saline CCC water encounters the warm and more-saline water from the Kuroshio (Liao et al. 2018; Oey et al. 2014).

As the Taiwan Strait is a subtropical strait connecting two marginal seas, the SST anomaly in this strait (hereinafter, referred to as TS-SSTa) exhibits the largest temporal variability along the China coastal seas. Similarly, our previous work suggested that signal of the temperature variability can be amplified in a strait connecting two neighboring seas, through the study of the heat transport between the Indo-Pacific Ocean and Southern Ocean (Liao et al. 2019). Several previous studies focused on the temporal variability characteristics of the SST in the China coastal seas, especially the Taiwan Strait. Oey et al. (2013) suggested that the warming of the eastern China coastal seas in the recent decades was associated with a stronger northeasterly wind and on-coast wind convergence from the open Pacific. Belkin and Lee (2014) reported three epochs of TS-SSTa multidecadal variations from 1957 to 2011, and the associated regime shifts occurred in 1976 and 1999. They also found that the long-term TS-SSTa variability is pronounced in winter, when the warming and cooling rates can be about +1 and -1 °C/decade before and after 1999. Wang and Oey (2014) attributed the TS-SSTa variability to the strengths of the sideways movements of the Kuroshio front to the northeast of Taiwan. Liao et al. (2015) further reported a relatively weak coastal warming trend in the low and mid-latitudes after 1998, including the China coastal seas. Moreover, the SST variability has serious consequences on the ecosystem of China coastal seas (Oey et al. 2018; Xu et al. 2013).

The Taiwan Strait is located at the boundary of the tropics and subtropics, and thus the local signal of the TS-SSTa variability can be significantly affected by the large-scale signals of PDO from subtropics and ENSO from tropics. Therefore, the Taiwan Strait is a good example to explore local responses to the large-scale climate signals. Meanwhile, it is necessary to assess the causes of TS-SSTa variability, especially considering the continuous threat of anthropogenic warming and increased abuse of coastal seas (Lima and Wethey 2012). However, several previous studies on the Taiwan Strait only focused on the extreme cold events and the local dynamics (e.g., Liao et al., 2013, 2018); Liao et al. (2015) reported the response of coastal SST in the low and mid-latitudes to global warming, while the effects of other climate signals were not involved. Therefore, contributions of the large-scale signals such as PDO and ENSO on the TS-SSTa variability have not been comprehensively analyzed as yet. That is largely due to insufficient work to

connect the local signals in the Taiwan Strait to those large-scale signals. (Liao et al., 2013).

The Pacific Ocean is mainly controlled by the large-scale climate signals of ENSO (Wang and Picaut 2002), PDO (Wang et al. 2008), global warming (Liao et al. 2015), NPO (Rogers 1981), and NPGO (Di Lorenzo et al. 2008). As aforementioned, NPO/NPGO is closely connected with PDO and ENSO. Therefore, it is reasonable to assume that the large-scale signals of ENSO, PDO, and global warming mainly impact the SST variability in the Northwestern Pacific, especially the Taiwan Strait. Therefore, we explored the contributions of these signals on the TS-SSTa variability based on their typical timescales in this study. Different period filters were applied to extract the different signals within the long-term TS-SSTa data. Using this method, the present study demonstrates the complicated connections between the TS-SSTa variability and the large-scale signals, within which the modulation of PDO on the TS-SSTa variability is relatively novel and has not been clearly reported before. The remainder of this manuscript is organized as follows. Section 2 describes the observational datasets and analysis methods. Section 3 presents the TS-SSTa temporal variability and its correlations with the PDO/ENSO. Section 4 describes the mechanisms that explain the PDO modulation of the PDO/ENSO–SST relationship. Finally, the results are discussed and summarized in Sects. 5 and 6, respectively.

## 2 Data and Methods

### 2.1 Data

Two SST datasets were used in this study. The first dataset is the monthly Optimum Interpolation SST data on a  $0.25^\circ \times 0.25^\circ$  grid from 1982 to 2021 (OISST, Reynolds and Chelton 2010). OISST has the advantage of relatively high horizontal resolution and can reflect the detailed spatial characteristics of the warming/cooling trends in the Taiwan Strait, as the study by Oey et al. (2013). However, it is temporally too short to analyze the interdecadal signal related to PDO. Hence, the second dataset we applied is the temporally longer UK Meteorological Office Hadley Centre SST climatology (HadISST) data, as the study by Belkin et al. (2014). It dates back to 1870, and has monthly temporal resolution and  $1^\circ \times 1^\circ$  spatial resolution (Rayner et al. 2003; Rayner et al. 2006).

Note that the hydrographic data density increased sharply in 1957, which was the International Geophysical Year (1957–1958). Therefore, the SST data from 1957 to 2021 were used to analyze the basin-scale relationship between the PDO and SST in this study (Belkin 2009; Belkin and

Lee 2014). Note also that the wintertime SST was constructed by averaging the monthly data of January, February, and March. In this paper, “SST” refers to the wintertime SST unless indicated otherwise.

The Niño3.4, PDO, and the North Pacific Oscillation (NPO)/North Pacific Gyre Oscillation (NPGO) indexes were obtained from the National Oceanic and Atmospheric Administration. The indexes averaged from December, January, and February were used in this study. Note that time series of these indexes were standardized by dividing each series by their corresponding standard deviations.

Furthermore, the monthly sea level pressure (SLP,  $2.5^\circ \times 2.5^\circ$  gridded), surface wind ( $2.5^\circ \times 2.5^\circ$  gridded), and surface air temperature (SAT,  $2.5^\circ \times 2.5^\circ$  gridded) data from 1948 to 2021 were obtained from the National Centers for Environmental Prediction (NCEP) to explore the mechanism of large-scale climate signals on local signals.

## 2.2 Methods

In this study, the temporal variability signals related to ENSO, PDO, and global warming were isolated using different filters based on their typical timescales. Firstly, ENSO is generally considered to have an interannual quasi-period of 2–7 years (Wang and Picaut 2002). Therefore, an 8-year high-pass filter was reasonably used to obtain the ENSO-related interannual signal (Liu and Di Lorenzo 2018). Note that a 4-year high-pass filter was also applied to further demonstrate the interannual variability with higher frequency; Secondly, as shown in Fig. S1, the PDO waxes and wanes approximately every 15 to 30 years, indicating an interdecadal period of about 30–60 years (Wang et al. 2008). Hence, an 8–60-year band-pass filter was applied to preserve the interdecadal signal related to PDO. Note that for the relatively short OISST (1982–2021), a 8-year low-pass filter was sufficient to derive its interdecadal signal related to PDO; Thirdly, as noted in Schlesinger and Ramankutty (1994), the signal of global warming is usually regarded as a low-frequency signal with a period of 65–70 years, rather than just a linear trend. Therefore, a 60-year low-pass filter can effectively filter out the signal related to

global warming. Note that the slightly different filters gave qualitatively similar results for the following analyses.

In addition, Morlet wavelet analysis was performed to demonstrate the temporal variation of the TS-SSTa power spectrum (Torrence and Compo 1998). Morlet wavelet analysis has the advantage of demonstrating the temporal variation of the TS-SSTa power spectrum. Hence, it can present the TS-SSTa power spectrum during different PDO phase periods, highlighting the modulation of PDO on the PDO/ENSO–SST relationship. The TS-SSTa time series was standardized by dividing it by its standard deviation before the wavelet analysis. Meanwhile, the interannual component of the SST variation is calculated as the integral of the wavelet power with period less than 8 years divided by the total power from 1957 to 2017.

## 3 Results

### 3.1 TS-SSTa Trends and Correlations with the PDO/ENSO

The SST anomaly (SSTa, from OISST) in the China coastal seas shows a significant warming trend from 1982 to 1999 (Fig. 1a) and a cooling trend from 1999 to 2014 (Fig. 1b). This SSTa trend is especially strengthened in the Taiwan Strait (Fig. 1). During the warming period, the TS-SSTa increases at a rate of  $1.20 \text{ }^\circ\text{C/decade}$  ( $p < 0.01$ , Fig. 1c; Table 1). The area of the strongest warming is located on the western side of the Taiwan Strait, with a maximum warming rate of  $2.78 \text{ }^\circ\text{C/decade}$ . On the other hand, during the cooling period, relatively less coastal areas experienced significant cooling (Fig. 1b). The TS-SSTa decreases at a rate of  $-0.80 \text{ }^\circ\text{C/decade}$  ( $p < 0.01$ , Fig. 1c; Table 1). The strongest cooling region occurs on the western side of the Taiwan Strait, and the maximum cooling rate is  $-2.20 \text{ }^\circ\text{C/decade}$ . The co-occurrence of the maximum warming and cooling trends in the western Taiwan Strait indicates the potential role of the CCC on the TS-SSTa temporal variability. As the CCC depends strongly on the strength of the EAWM, the TS-SSTa variability may also be related in part to the large-scale atmospheric variability of the EAWM.

**Table 1** Trends of the area-averaged Taiwan Strait sea surface temperature anomaly (TS-SSTa) and the interannual (8-year high-pass filtered), interdecadal (8–60-year band-pass filtered), and long-term (60-year low-pass filtered) TS-SSTa during the warming and cooling periods, i.e., before and after 1999. The percentages in bold show the contributions of the different signals to the SST trend

Unit: $^\circ\text{C/decade}$	1982–1999 (warming)	1999–2014 (cooling)
TS-SSTa (OISST)	$1.20$ ( $p < 0.01$ )	$-0.80$ ( $p < 0.01$ )
TS-SSTa (HadISST)	$1.02$ ( $p < 0.01$ , <b>100%</b> )	$-0.49$ ( $p = 0.04$ , <b>100%</b> )
Interannual TS-SSTa (HadISST)	$0.08$ ( $p = 0.55$ , <b>8%</b> )	$0.02$ ( $p = 0.91$ , <b>-4%</b> )
Interdecadal TS-SSTa (HadISST)	$0.42$ ( $p < 0.01$ , <b>41%</b> )	$-0.31$ ( $p = 0.05$ , <b>63%</b> )
Long-term TS-SSTa (HadISST)	$0.52$ ( $p < 0.01$ , <b>51%</b> )	$-0.20$ ( $p < 0.01$ , <b>41%</b> )

As noted by Kim et al. (2017); Wang et al. (2000), the EAWM may be affected by the ENSO primarily through an anomalous low-tropospheric anticyclonic/cyclonic circulation over the western North Pacific. Therefore, the El Niño years are supposed to be accompanied by warming in East Asia, whereas the La Niña years are accompanied by cooling in East Asia. However, the situation appears to be different in the Taiwan Strait. As shown in Fig. 2a, the TS-SSTa is not correlated with the ENSO ( $R = -0.04, p = 0.83$ , Table 2), but it has a significant negative correlation with the PDO ( $R = -0.43, p < 0.01$ , Table 2). Likewise, the interdecadal TS-SSTa (8-year low-pass filtered) is significantly anticorrelated with the PDO ( $R = -0.47, p < 0.01$ , Fig. 2b; Table 2),

while the interannual TS-SSTa (8-year high-pass filtered) shows no correlation with the ENSO ( $R = -0.01, p = 0.94$ , Fig. 2c; Table 2). However, a positive correlation ( $R = 0.64, p = 0.12$ , Table 2) exists between the interannual TS-SSTa and ENSO from 2007 to 2013, which is a short period of the negative PDO phase. This finding suggests that the PDO possibly modulates the relationship between the TS-SSTa and ENSO on the interdecadal timescale. However, the OISST data are not sufficiently long (1982–2021) to regard the 8-year low-pass filtered TS-SSTa as an interdecadal signal. Therefore, the interdecadal modulation of the PDO on the relationship between TS-SSTa and ENSO was further analyzed using the longer HadISST data, as described in Sect. 3.2.

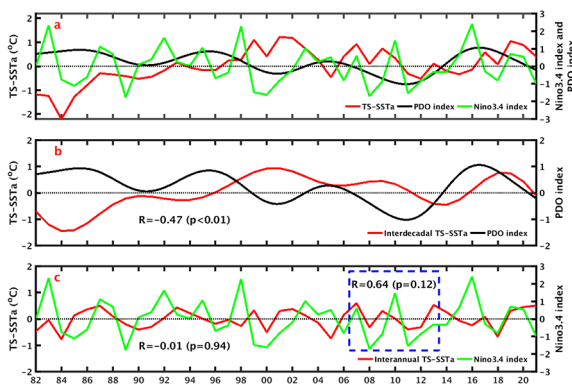


**Fig. 2** (a) Time series of the TS-SSTa (from OISST, red solid line, same as in Fig. 1c), the Pacific Decadal Oscillation (PDO) index (8-year low-pass filtered, black solid line), and the Niño3.4 index (green solid line). (b) Time series of the interdecadal TS-SSTa (8-year low-pass filtered, red solid line) and the PDO index (8-year low-pass filtered, black solid line). (c) Time series of the interannual TS-SSTa (8-year high-pass filtered, red solid line) and the Niño3.4 index (green solid line). The blue dashed box shows a period of negative PDO phase from 2007 to 2013

The spatial distributions of the SST–ENSO and SST–PDO correlation coefficients in the western North Pacific from 1982 to 2021 are shown in Fig. 3. Figure 3a shows the positive and negative correlations between the SST and ENSO in the eastern and western equatorial Pacific, respectively, reflecting the influence of ENSO on the SST in the Pacific Ocean. Similar to the observations made from Fig. 2a, no SST–ENSO correlation is found in the Taiwan Strait (see the magnified view in Fig. 3c); While in Fig. 3b, the SST is negatively correlated with the PDO in most western North Pacific, including China coastal seas from southern East China Sea to the northern South China Sea, especially the Taiwan Strait (see the magnified view in Fig. 3d). The SST and PDO are significantly correlated along the path of the Kuroshio. It is interesting that the regions with significant SST–ENSO and SST–PDO correlations seem to be spatially complementary in the China coastal seas (Fig. 3c and d). In addition, the area of the regions with significant SST–PDO correlation exceeds that with SST–ENSO correlation (Fig. 3c and d), indicating that the SST temporal variability

**Table 2** Correlation and regression coefficients between TS-SSTa and the Pacific Decadal Oscillation/El Niño–Southern Oscillation (PDO/ENSO) index. The OISST data are from 1982 through 2021, and HadISST data are from 1957 through 2021. Values that pass the 95% significance test are shown in bold

OISST	1982–2021 (mostly in positive PDO phase)	
TS-SSTa vs. PDO	<b>-0.43</b> ( $p < 0.01$ )	
TS-SSTa vs. ENSO	-0.04 ( $p = 0.83$ )	
TS-SSTa (8-year low-pass) vs. PDO	<b>-0.47</b> ( $p < 0.01$ )	
TS-SSTa (8-year high-pass) vs. ENSO	-0.01 ( $p = 0.94$ )	
TS-SSTa (8-year high-pass) vs. ENSO	0.64 ( $p = 0.12$ , from 2007 to 2013)	
	Positive PDO phase	Negative PDO phase
HadISST (correlation coefficient $R$ )		
TS-SSTa (8–60-year band-pass) vs. PDO	<b>-0.64</b> ( $p < 0.01$ )	0.06 ( $p = 0.77$ )
TS-SSTa (8-year high-pass) vs. ENSO	0.31 ( $p = 0.10$ )	<b>0.36</b> ( $p = 0.02$ )
TS-SSTa (4-year high-pass) vs. ENSO	0.17 ( $p = 0.37$ )	<b>0.58</b> ( $p < 0.01$ )
HadISST (regression coefficient $Rr$ )		
TS-SSTa (8–60-year band-pass) to PDO	<b>-0.43</b> ( $p < 0.01$ )	-0.10 ( $p = 0.77$ )
TS-SSTa (8-year high-pass) to ENSO	0.08 ( $p = 0.10$ )	<b>0.16</b> ( $p = 0.02$ )
TS-SSTa (4-year high-pass) to ENSO	0.03 ( $p = 0.37$ )	<b>0.13</b> ( $p < 0.01$ )

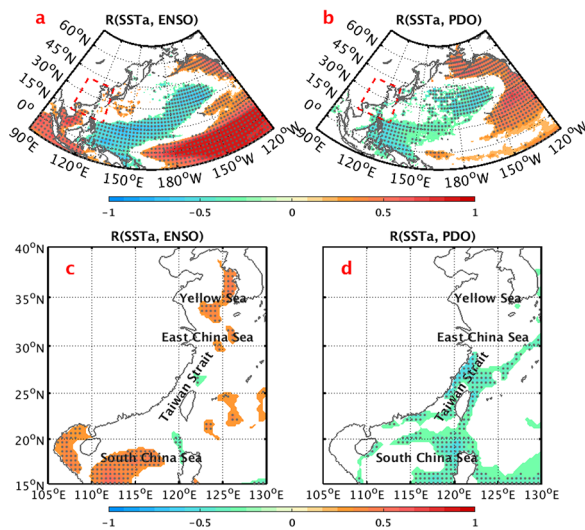


**Fig. 3** (a, b) Spatial distributions of the correlation coefficients (a) between SST anomaly (from OISST data) and the El Niño–Southern Oscillation (ENSO), as well as (b) between the SST anomaly and the PDO, in the North Pacific from 1982 to 2021. (c, d) A magnified view of the region of the China coastal seas (red dashed box) in (a, b), respectively. Color shading and gray points represent correlations at the 90% and 95% significance levels, respectively

in the China coastal seas is dominated by the PDO from 1982 to 2021.

### 3.2 Modulation of PDO on the Relationship between TS-SSTa and PDO/ENSO

To further demonstrate the interdecadal modulation of the PDO on the TS-SSTa–PDO/ENSO relationship, the longer HadISST data from 1957 to 2021 were used. As shown in Fig. 4, the TS-SSTa time series was divided into three components: the interannual variation related to ENSO (8-year high-pass filtered), interdecadal variation related to PDO (8–60-year band-pass filtered), and long-term variability related to global warming (60-year low-pass filtered), based on the filtering methods described in Sect. 2.2. Figure 4a shows consistent long-term variability between the wintertime TS-SSTa and the wintertime global mean SST anomaly, testifying that the long-term variability of the TS-SSTa is related to global warming. Meanwhile, the TS-SSTa from HadISST also shows significant warming and cooling trends during the periods 1982–1999 and 1999–2014, respectively; however, their values differ slightly from the corresponding trends seen in the OISST data. The long-term variability of TS-SSTa significantly contributed to its warming (+0.52/+1.02) and cooling (−0.20/−0.49) rates during 1982–1999 and 1999–2014, respectively (see Table 1). As aforementioned, it is assumed that the Northwestern Pacific, including the Taiwan Strait, is mainly impacted by

large-scale signals of ENSO, PDO, and global warming. Hence, the remaining interannual and interdecadal variations of the TS-SSTa are related to ENSO and PDO, respectively, due to their consistent timescales. These relations will be discussed further in the following sections.

According to the PDO index, we define 1957–1977 as the negative PDO phase period, 1978–2006 as the positive PDO phase period, and the short period of 2007–2013 is in the negative PDO phase period. For the whole period of 1957–2021, the interdecadal TS-SSTa and PDO are not correlated ( $R = -0.06$  ( $p = 0.65$ , Fig. 4c); the 4-year high-pass filtered interannual TS-SSTa is also weakly correlated with the ENSO with a correlation coefficient  $R$  of 0.36 ( $p = 0.02$ , Fig. 4d). Note that we used the 4-year high-pass filtered interannual TS-SSTa here, and the 8-year high-pass filtered interannual TS-SSTa gives qualitatively similar results. However, it is important to note that the relationship between the TS-SSTa and PDO/ENSO can be strongly influenced by the PDO phase, as demonstrated earlier using the OISST data. From Table 2, when the PDO is in its positive phase, the interdecadal TS-SSTa is significantly anticorrelated with the PDO ( $R = -0.64$ ,  $p < 0.01$ ), with a relatively large regression coefficient of  $-0.43$  ( $p < 0.01$ ) (notice that all the values are normalized); In contrast, the 4-year high-pass filtered interannual TS-SSTa is not correlated with the ENSO

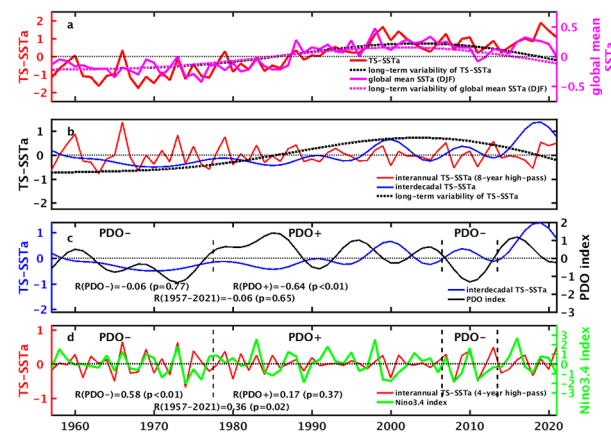


**Fig. 4** (a) Time series of the TS-SSTa (from HadISST, red solid line), the long-term variability of the TS-SSTa (60-year low-pass filtered, black dashed line), the wintertime global mean SST anomaly (magenta solid line, left scale) and the long-term variability of the wintertime global mean SST anomaly (magenta dashed line, left scale) from 1957 to 2021. (b) Time series of the interannual TS-SSTa (8-year high-pass filtered, red solid line), interdecadal TS-SSTa (8–60-year band-pass filtered, blue solid line), and the long-term variability (60-year low-pass filtered, black dashed line) of the TS-SSTa from 1957 to 2021. (c) Time series of the interdecadal TS-SSTa (8–60-year band-pass filtered, blue solid line), and the PDO index (8–60-year band-pass filtered, black solid line) from 1957 to 2021. (d) Time series of the interannual TS-SSTa (4-year high-pass filtered, red solid line), and the Niño3.4 index (green solid line) from 1957 to 2021

( $R=0.17, p=0.37$ ), with a weak regression coefficient of 0.03 ( $p=0.37$ ). However, when the PDO is in its negative phase, the interdecadal TS-SSTa is not correlated with the PDO ( $R=0.06, p=0.77$ ), and the associated regression coefficient is relatively small ( $Rr=-0.10, p=0.77$ ); In contrast, the 4-year high-pass filtered interannual TS-SSTa is significantly correlated with the ENSO ( $R=0.58, p<0.01$ ), with a relatively strong response ( $Rr=0.13, p<0.01$ ).

Moreover, Fig. 5a shows that the 11-year moving correlation coefficient between the 4-year high-pass filtered interannual TS-SSTa and ENSO is negatively correlated with the PDO ( $R=-0.51, p<0.01$ ) on the interdecadal timescale, i.e., the correlation between the TS-SSTa and ENSO is significant in the negative PDO phase and vice versa. The wavelet analysis shown in Fig. 5b and c indicates that the interannual signal (period less than 4 years) of the TS-SSTa related to ENSO increases significantly during the negative PDO phase period (blue solid line in Fig. 5c), as compared with the positive PDO phase period (red solid line in Fig. 5c). Above all, these statistics demonstrate clearly that the PDO phase can modulate the power spectrum of TS-SSTa, and therefore the response of TS-SSTa to the PDO/ENSO on the interdecadal timescale. To be specific, during the positive PDO phase period, the TS-SSTa has a strong interdecadal signal and a significant negative correlation with the PDO; In contrast, during the negative PDO phase period, the interannual signal dominates the TS-SSTa, which has a significant positive correlation with the ENSO.

The spatial distributions of the SST-ENSO and SST-PDO correlation coefficients during the different PDO

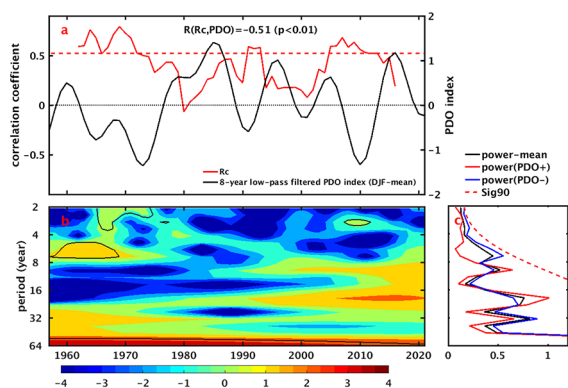


**Fig. 5** (a) Time series of the 11-year moving correlation coefficient ( $R_c$ ) between the 4-year high-pass filtered interannual TS-SSTa and ENSO (red solid line, scale on the left axis), and the interdecadal PDO index (8–60-year band-pass filtered, black solid line, scale on the right axis). (b) The Morlet wavelet power spectrum of the standardized TS-SSTa. The contours show the 90% significance level. (c) The time-averaged wavelet power spectrum for the positive (red solid line) and negative (blue solid line) PDO phase periods and for the whole period of 1957–2021 (black solid line). The red dashed line shows the 90% significance level

phases in the North Pacific from 1957 to 2021 are shown in Fig. 6. As mentioned in Fig. 4, during the positive PDO phase period, the interdecadal SST is highly anticorrelated with the PDO in the western North Pacific, especially in the China coastal seas (Fig. 6a). However, this correlation vanishes during the negative PDO phase period (Fig. 6b). On the other hand, although the interannual SST is significantly correlated with the ENSO in the low latitudes, this area of credible correlation is not observed in the China coastal seas during the positive PDO phase period (Fig. 6c). During the negative PDO phase period, the correlation between the interannual SST and ENSO becomes more significant and

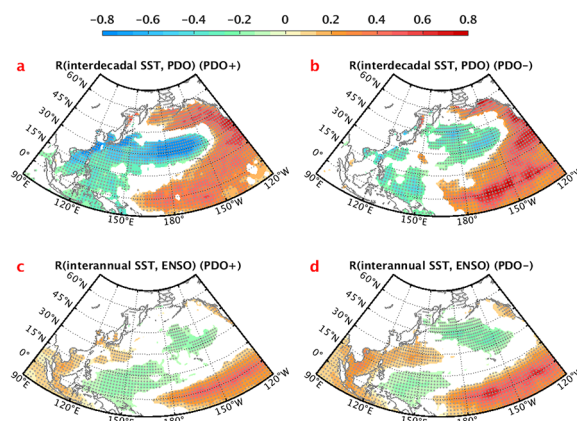


**Fig. 6** (a, b) Spatial distributions of the correlation coefficients between the interdecadal SST (8–60-year band-pass filtered) and the PDO during the positive (a) and negative (b) PDO phases in the North Pacific. (c, d) Spatial distributions of the correlation coefficients between the interannual SST (8-year high-pass filtered) and ENSO during the positive (c) and negative (d) PDO phases in the North Pacific. Color shading and gray points represent correlations at the 90% and 95% significance levels, respectively

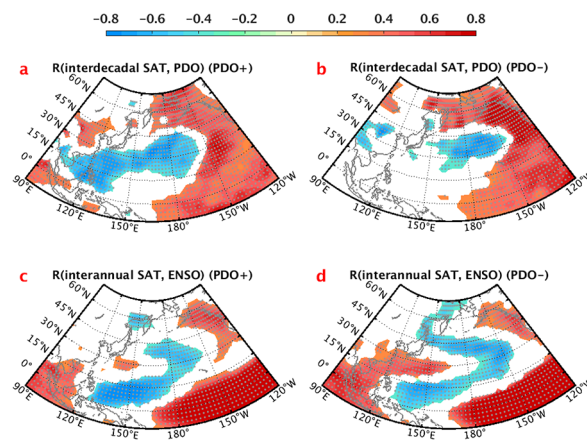


**Fig. 7** Same as Fig. 6, but for National Centers for Environmental Prediction (NCEP) surface air temperature (SAT)

extends to the Taiwan Strait (Fig. 6d). Similar results can be derived using the NCEP SAT data from 1948 to 2021 (Fig. 7). Along the Chinese coast and especially in the Taiwan Strait, the interdecadal SAT has a significant anticorrelation with the PDO during the positive PDO phase period (Fig. 7a), and the interannual SAT is highly correlated with the ENSO during the negative PDO phase period (Fig. 7d). Note that the variabilities of the SST and SAT are highly consistent, especially in the middle and low latitudes (figures not shown). Consistently, the interannual component of the SST variation related to the ENSO is relatively small in the western North Pacific during the positive PDO phase period (Fig. 8a), whereas it is highly strengthened and extended when the PDO is in its negative phase, especially in the China coastal seas (Fig. 8b and c).

From the above analysis, we can conclude that along the Chinese coast and especially in the Taiwan Strait, the PDO has a dominating influence on the SST/SAT variability on the interdecadal timescale during the positive PDO phase period, whereas the interannual component of the SST/SAT variability is strengthened and dominated by the ENSO during the negative PDO phase period. In a word, PDO can significantly change the power spectrum of the TS-SSTa and thus modulate the relationship between TS-SSTa and PDO/

ENSO. The PDO and ENSO alternately control the TS-SSTa variability according to the PDO phases. Therefore, the warming and cooling trend in the Taiwan Strait during 1982–2014 (mostly in positive PDO phase) is mainly contributed by the interdecadal signal of the PDO and long-term signal of global warming. As listed in Table 1, PDO and global warming account for roughly 41% (+0.42/+1.02) and 51% (+0.52/+1.02) of the warming trend during 1982–1999; and 63% (−0.31/−0.49) and 41% (−0.20/−0.49) of the cooling trend during 1999–2014, respectively.

## 4 Possible Influencing Mechanisms by the PDO/ENSO

To further reveal the physical mechanisms of the influence of the PDO and ENSO on the SST temporal variability in the China coastal seas, especially in the Taiwan Strait, we examined the SST (HadISST), SLP (NCEP), and surface wind (NCEP) data from 1957 to 2021.

### 4.1 Influence of the PDO on TS-SSTa

The influence of the PDO on the TS-SSTa temporal variability is mainly evident on the interdecadal timescale during the positive PDO phase period (see Table 2). Figure 9a–d show the regression patterns of the SLP and surface wind anomalies with respect to the PDO in the North Pacific from 1957 to 2021. As shown in Fig. 6a, the interdecadal SST in most of the western North Pacific is significantly anticorrelated with the PDO during the positive PDO phase period. The corresponding SLP regression map shows a dipole with a positive SLP anomaly over the northeastern Eurasia and a negative SLP anomaly over the North Pacific (Fig. 9a). This SLP dipole can lead to a northeasterly wind jet anomaly along the eastern coast of the Eurasian continent, thereby influencing the EAWM and subsequently the SST variability in the western North Pacific, especially in the China coastal seas (Fig. 9c). In contrast, the interdecadal SST–PDO relationship disappears in the western North Pacific during the negative PDO phase period (Fig. 6b) because there is neither an SLP dipole in the north (Fig. 9b), nor a northeasterly wind jet anomaly along the eastern coast of the Eurasian continent (Fig. 9d). In other words, the PDO can significantly affect the TS-SSTa variability through the SLP dipole and its associated northeasterly wind jet anomaly in the western North Pacific on the interdecadal timescale during the positive PDO phase period. However, this process does not occur during the negative PDO phase period.

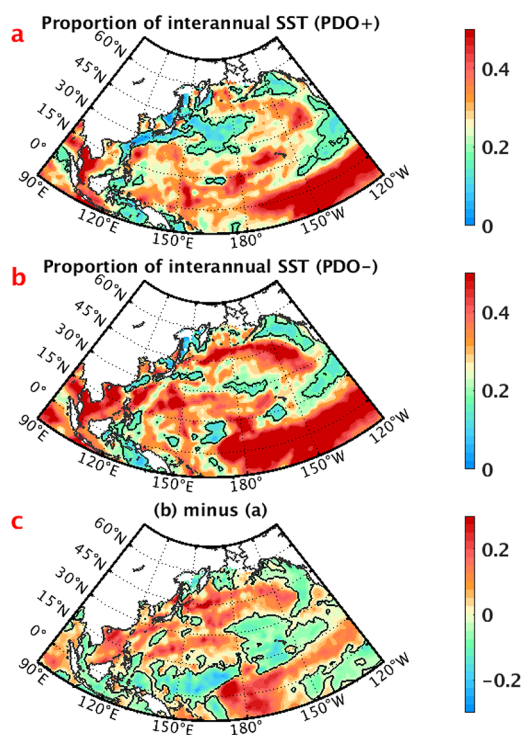


**Fig. 8** Interannual component of the SST variation based on the Morlet wavelet analysis during the positive (a) and negative (b) PDO phases. (c) Difference between (b) and (a) (b minus a). Contours indicate values of 0.25 (a and b) and 0 (c)

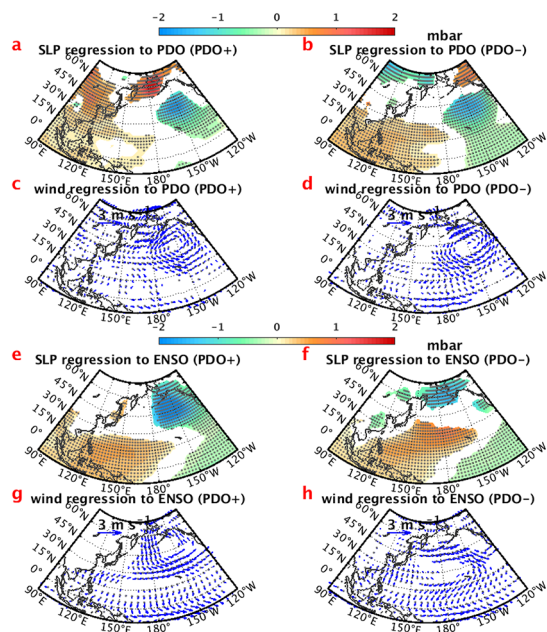


**Fig. 9** (a, c) Regression map of the interdecadal (8–60-year band-pass filtered) sea level pressure (SLP) (a) and surface wind anomalies (c) to the PDO during the positive PDO phase period (PDO+). (b, d) Same as (a, c), but during the negative PDO phase period (PDO–). (e, g) The regression map of the interannual (8-year high-pass filtered) SLP (e) and surface wind anomalies (g) to the ENSO during the positive PDO phase period (PDO+). (f, h) Same as (e, g), but during the negative PDO phase period (PDO–). Color shading and vectors indicate the 90% significance level. The gray points indicate the 95% significance level

## 4.2 Influence of the ENSO on TS-SSTa

The ENSO influences the TS-SSTa temporal variability mainly on the interannual timescale during the negative PDO phase period, as mentioned earlier (see Table 2). Figure 9e–h shows the corresponding regression patterns of the interannual SLP and surface wind anomalies with respect to the ENSO in the North Pacific from 1957 to 2021. The positive correlation between the interannual SST and ENSO is relatively weak in the China coastal seas and is confined to the region south of 30°N during the positive PDO phase period (Fig. 6c). The associated ENSO-regressed SLP and surface wind anomaly show an anomalous anticyclone south of 30°N in the lower troposphere over the western North Pacific (Fig. 9e and g). This anomalous anticyclone leads to a larger cross-shore component of the surface wind anomaly along the Chinese coast, especially in the Taiwan Strait (Fig. 9 g). However, this positive correlation between the interannual SST and ENSO in the China coastal seas strengthens significantly and extends northward beyond 30°N during the negative PDO phase period (Fig. 6d). Correspondingly, the associated SLP and surface wind anomaly

regression maps show a northward extension of the low-level anticyclone to roughly 45°N (Fig. 9f and h). This northward extension of the anticyclone induces a stronger surface wind anomaly with a larger along-shore component in the China coastal seas, especially in the Taiwan Strait (Fig. 9 h).

Figure 10 further demonstrates the differences in the ENSO-regressed SLP and its induced surface wind anomaly in different PDO phases. An anticyclone is clearly observed in the central North Pacific where the PDO is active, proving that the difference is mainly caused by the PDO (Fig. 10c). As noted above in Fig. 9, the response of the surface wind anomaly to the ENSO is stronger and has a larger along-shore component in the negative PDO phase (blue vectors) than in the positive PDO phase (red vectors) over the western North Pacific, including the China coastal seas (Fig. 10a). Therefore, the PDO can modulate the ENSO–EAWM relationship on the interdecadal timescale, with an on-shore surface wind pattern near the China coastal seas when the PDO phase undergoes a transition from negative to positive (Fig. 10b). The PDO-modulated ENSO-regressed EAWM variation drives the CCC and thus modifies the TS-SSTa temporal variability. A schematic based on the above results is shown in Fig. 10d, and it shows the response of the EAWM variation to the ENSO near the Taiwan Strait during the positive and negative PDO phase periods. During the positive PDO phase period, the ENSO-regressed EAWM variation is relatively weak and shows a larger cross-shore component (the shorter red vector). It has little effect on the along-shore currents (e.g., CCC) in the Taiwan Strait. Thus, the response of TS-SSTa variability to the ENSO is not significant. In contrast, during the negative PDO phase period, the response of the EAWM variation to the ENSO is more significant. A correspondingly stronger surface wind anomaly shows a larger along-shore component (the longer blue vector), which has strong effect on the along-shore currents in the Taiwan Strait and thus the TS-SSTa variability. In particular, the southward intrusion of the cold water into the Taiwan Strait by CCC is hindered during El Niño but enhanced during La Niña.

## 5 Discussion

### 5.1 Oceanic influence of the NPO/NPGO on TS-SSTa

#### 5.1.1 Interdecadal influence of the PDO-related NPO/NPGO on TS-SSTa

PDO can significantly influence the TS-SSTa variability on the interdecadal timescale through two paths. The first one is the atmospheric path. As described above in Sect. 4.1,

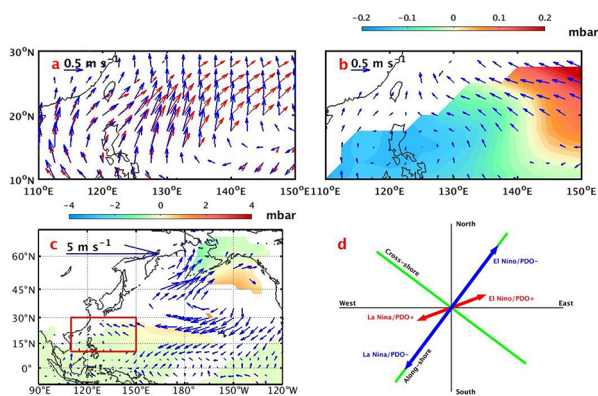


**Fig. 10** (a) ENSO-regressed surface wind anomaly during the positive (red vectors, same as Fig. 9 g) and negative (blue vectors, same as Fig. 9 h) PDO phase periods in parts of East Asia and Western Pacific (110°E–150°E, 10°N–30°N, the red solid box area in c). (b) The differences in the ENSO-regressed SLP (color shading, subtracting the values in Fig. 9 e from those in Fig. 9 f) and the surface wind anomaly (vectors, subtracting the values in Fig. 9 g from those in Fig. 9 h) for the different PDO phases. (c) Same as (b) but over the North Pacific. Color shading and vectors indicate the 90% significance level. (d) Schematic of the response of the surface wind anomaly to the ENSO during the positive (red vectors) and negative (blue vectors) PDO phase periods in the Taiwan Strait. The green lines indicate the along-shore and cross-shore directions

during the positive PDO phase period, the PDO-regressed SLP shows a dipole over the North Pacific (Fig. 9a), leading to the formation of a northeasterly wind jet anomaly along the eastern coast of the Eurasian continent (Fig. 9c). This wind jet anomaly influences the EAWM and subsequently the SST variability in the western North Pacific, including in the Taiwan Strait; The second one is the oceanic path. The PDO-regressed SLP dipole over the North Pacific also describes the signal of the NPO (Fig. 9a). The NPO induces a northeasterly wind jet anomaly along the eastern coast of the Eurasian continent (Fig. 9c), and this anomaly affects the variability of NPGO, especially the Kuroshio and North Pacific Warm Current (Jiang et al. 2013). Hence, the SST along the path of the Kuroshio and North Pacific Warm Current, including in the Taiwan Strait, decreases (Fig. 6a).

This oceanic path related to NPO/NPGO is mainly discussed in this sub-Section. Figure 11a shows that the NPGO has no significant correlation with the PDO from 1950 to 1977 (the negative PDO phase period,  $R=0.00$ ,  $p=0.98$ ), while there is a significant anticorrelation between the NPGO and PDO on the interdecadal timescale from 1978 to 2021 (mostly in the positive PDO phase period,  $R=-0.35$ ,  $p=0.06$ ). Similarly, Fig. 11b demonstrates that there is no significant correlation ( $R=0.15$ ,  $p=0.38$ ) between the NPGO and interdecadal TS-SSTa during the negative PDO phase, while their correlation coefficient reaches 0.60 ( $p<0.01$ ) during the positive PDO phase. Consequently, the

PDO-related NPGO can significantly influence the TS-SSTa variability on the interdecadal timescale from 1978 to 2014 (mostly in the positive PDO phase period), but not during the negative PDO phase period.

Possible mechanisms are proposed as follows. As presented in Fig. 11c, during the positive PDO phase period, the NPO-related SLP dipole is significant with the strong Aleutian Low occupying the North Pacific. Both the PDO and NPGO are controlled by the strength of Aleutian Low, and thus the NPGO mainly presents interdecadal signal (Fig. 11a and b, after 1977/1978). The northeasterly wind jet anomaly forced by the SLP dipole suppresses the North Pacific Gyre, thereby slowing down the Kuroshio and thus affecting the SST variability in the China coastal seas, especially the Taiwan Strait; In contrast, as presented in Fig. 11d, during the negative PDO phase period, the Aleutian Low weakens and withdraws to the northwestern North Pacific (Hook et al. 2015). The North Pacific High located at the Northeastern Pacific becomes dominant in the North Pacific. Therefore, the NPGO is mainly controlled by the dipole composed of weakened Aleutian Low and North Pacific High. The NPGO mainly presents interannual signals (Fig. 11a and b, before 1977/1978). In brief, the PDO-related NPO/NPGO can significantly influence the TS-SSTa variability on the interdecadal timescale during the positive PDO phase period, but not during the negative PDO phase period.

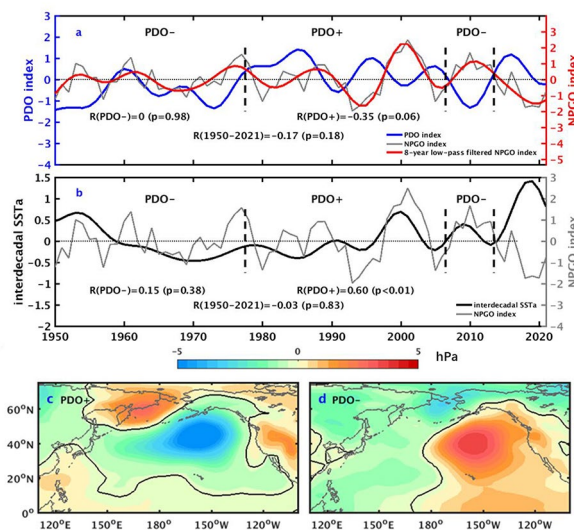


**Fig. 11** (a) Correlations between the PDO and NPGO indexes from 1950 to 2021. (b) Correlations between the interdecadal TS-SSTa and NPGO index from 1950 to 2021. (c, d) Composite map of the sea level pressure (SLP) anomaly for positive PDO years (c, 1961, 1984, 1987, 1995, 1997, and 2015) and negative PDO years (d, 2000, 2002, 2008, 2009, and 2011)

### 5.1.2 Interannual influence of the ENSO-related NPO/NPGO on TS-SSTa

In addition, ENSO-related NPO/NPGO can also influence the TS-SSTa variability on the interannual timescale through the oceanic path. Di Lorenzo et al. (2010) reported that the NPGO is closely related to ENSO, specifically the central Pacific El Niño. The ENSO-regressed SLP shows an NPO-like dipole structure over the North Pacific during the negative PDO phase period (Fig. 9f). This SLP dipole develops when the Aleutian Low is confined to the northern North Pacific and the North Pacific High extends northward to nearly 45°N on the interannual timescale; In contrast, this interannual SLP dipole is not significant during the positive PDO phase period (Fig. 9e) because the associated Aleutian Low occupies most of the North Pacific, suppressing the northward extension of the North Pacific High. Consequently, the ENSO-related NPO/NPGO affect the TS-SSTa variability on an interannual timescale during the negative PDO phase period but not during the positive PDO phase period.

In all, when the Aleutian Low occupies the North Pacific during the positive PDO phase period, the PDO-related NPO/NPGO significantly influences the TS-SSTa variability on the interdecadal timescale (Fig. 12a); In contrast, when the North Pacific High occupies the North Pacific during the negative PDO phase period, the ENSO-related NPO/NPGO significantly influences the TS-SSTa variability on the interannual timescale (Fig. 12b). However, the impacts of PDO and ENSO-related NPO/NPGO on the TS-SSTa variability, and the associated mechanisms are more complicated and needs further study.

Furthermore, the SST variability in the China coastal seas may also be influenced by the Arctic Oscillation (Wang and Ikeda 2000), Arctic Sea ice coverage (Parkinson et al. 2006), the Atlantic Multidecadal Oscillation (Levine et al. 2017), etc. Their impacts on the TS-SSTa variability should be relatively weaker compared with those depicted in the present study (e.g., PDO and ENSO), which would be investigated further in our future studies.

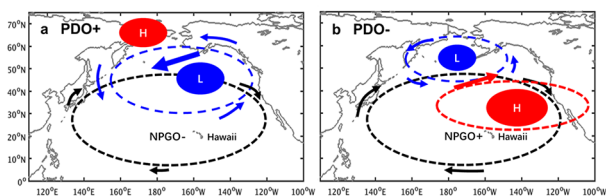


**Fig. 12** Schematic diagram of the North Pacific Oscillation (NPO) and NPGO during positive (a) and negative (b) PDO phase periods. L denotes the low SLP, and H denotes the high SLP

### 5.2 Shortening of the PDO period in recent decades

It is found that the aforementioned relationship between PDO and TS-SSTa is relatively weaker in recent decade. It may be because that PDO presents a relatively long cycle period of about 30–60 years (roughly 1943–1977 for negative PDO phase and 1978–2006 for positive PDO phase) before 2006; while a short period of about 10 years (roughly 2007–2013 for negative PDO phase and 2014–2020 for positive PDO phase) after 2006 (Fig. S1). This high-frequency oscillation of PDO makes it difficult to distinguish the TS-SSTa variabilities caused by the PDO and ENSO. Therefore, the impacts of PDO and ENSO on the TS-SSTa variability in recent decades can be more complicated, which is beyond the focus of this study and worthy to be explored in the future.

### 5.3 Local extreme events

Extreme cold events often occur in the winter Taiwan Strait (Chang et al. 2009; Cheng and Chang 2018; Hsieh et al. 2008; Lee et al. 2014), and even cause serious cold disasters (Liao et al. 2013). Large-scale climate change has been proved to have a far-reaching impact on local extreme events, such as flood and drought (Ehteram et al. 2018; Sharafati and Pezeshki 2020; Zhao et al. 2018). Based on this study, the PDO can modified the role of ENSO on SST in the Taiwan strait, the latter could trigger the extreme events there. Combined with numerical model simulations, the mechanisms proposed in this study will be used to predict the occurrence of extreme cold events in the Taiwan Strait in our future work.

## 6 Conclusions

The Taiwan Strait exhibits the largest SST temporal variability along the Chinese coast. The TS-SSTa presents significant increasing and decreasing trends during the periods 1982–1999 and 1999–2014, respectively, during which the PDO is almost in its positive phase. The TS-SSTa trends can be mainly attributed to two signals of different timescales: the interdecadal variability related to the PDO, and long-term variability associated with the global warming. The PDO and global warming accounted for 41% and 51% of the warming trend, and 63% and 41% of the cooling trend in the Taiwan Strait, respectively.

On the one hand, PDO and ENSO can influence the TS-SSTa variability through the atmospheric path of impacting the EAWM. PDO modulates the power spectrum of the TS-SSTa and thus the relationship between TS-SSTa and PDO/ENSO. As a result, PDO and ENSO alternately control the

TS-SSTa variability according to the different PDO phases. During the positive PDO phase period, PDO has a dominating influence on the TS-SSTa variability on the interdecadal timescale. The PDO-regressed SLP anomaly shows a dipole with a positive SLP anomaly over the northeastern Eurasia and a negative SLP anomaly over the North Pacific. It leads to the formation of a northeasterly wind jet anomaly along the eastern coast of the Eurasian continent, influencing the EAWM and subsequently the SST variability in the western North Pacific. In contrast, during the negative PDO phase period, ENSO has a dominating influence on the TS-SSTa variability on the interannual timescale. The ENSO-regressed SLP and surface wind anomaly are manifested as an anticyclone extending northward to roughly 45°N in the lower troposphere over the western North Pacific. The corresponding ENSO-regressed surface wind anomaly is stronger and shows a larger along-shore component near the Taiwan Strait, and thereby it easily affects the EAWM and thus the TS-SSTa variability.

On the other hand, PDO and ENSO-related NPO/NPGO can impact TS-SSTa variability through the oceanic path. When the Aleutian Low occupies the North Pacific during the positive PDO phase period, the PDO-related NPO/NPGO significantly influences the TS-SSTa variability on the interdecadal timescale; In contrast, when the North Pacific High occupies the North Pacific during the negative PDO phase period, the ENSO-related NPO/NPGO significantly influences the TS-SSTa variability on the interannual timescale.

However, more elaborate work shall be addressed in future study. Firstly, the influences of PDO and ENSO on the TS-SSTa variability during the recent decades of the high-frequency PDO oscillation are worthy to be further explored; Secondly, more robust evidences are required for the mechanisms of PDO and ENSO-related NPO/NPGO impacting the TS-SSTa variability; Thirdly, the influences of other large-scale signals (e.g., Arctic Oscillation, Atlantic Multidecadal Oscillation, etc.) on the TS-SSTa variability needs further study; Fourthly, the mechanisms proposed in this study can be testified using numerical model simulations, which can also be applied to predict the occurrence of extreme cold events in the Taiwan Strait. These problems will be addressed in our future works.

**Supplementary Information** The online version contains supplementary material available at <https://doi.org/10.1007/s00382-022-06270-9>.

**Acknowledgements** This work was supported by the Chinese Ministry of Science and Technology through the National Key Research and Development Program of China (2018YFC1407502), and grant (U1805241,41876004) from Natural Science Foundation of China.

**Data Availability** The OISST data are obtained from the following web

site: <https://www.ncdc.noaa.gov/oisst>. Monthly HadISST data can be accessed from the following web site: <https://www.metoffice.gov.uk/hadobs/hadisst/>. The Niño3.4 index data are obtained from the web site [https://psl.noaa.gov/gcos\\_wgsp/Timeseries/Data/nino34.long.anom.data](https://psl.noaa.gov/gcos_wgsp/Timeseries/Data/nino34.long.anom.data). The PDO index data are retrieved from the JISAO from the following web site: [https://psl.noaa.gov/gcos\\_wgsp/Timeseries/Data/pdo.long.data](https://psl.noaa.gov/gcos_wgsp/Timeseries/Data/pdo.long.data). Monthly SLP, sea surface wind, and SAT data are provided by the NCEP and accessed from their website: <https://psl.noaa.gov/data/gridded/data.-ncep.reanalysis.html>. The NPO/NPGO index data are obtained from the following web site: <http://www.oces.us/npgo/npgo.php>.

**Significance Statement** Wintertime sea surface temperature along the coast of China exhibits the largest temporal variability in the Taiwan Strait. We propose a mechanism to explain how the PDO and ENSO alternately control the sea surface temperature in the Taiwan Strait in different PDO phases under the background of global warming. This mechanism can help predict the sea surface temperature trend along the western coast of the North Pacific and can be useful to explain the occurrence of extreme warm and cold events in such a typical subtropical strait.

**Statements and Declarations** All authors certify that they have no affiliations with or involvement in any organization or entity with any financial interest or non-financial interest in the subject matter or materials discussed in this manuscript.

## References

- Alexander MA, Blade I, Newman M, Lanzante JR, Lau NC, Scott JD (2002) The atmospheric bridge: The influence of ENSO teleconnections on air-sea interaction over the global oceans. *J Clim* 15:2205–2231
- Annamalai H, Liu P, Xie SP (2005) Southwest Indian Ocean SST variability: Its local effect and remote influence on Asian monsoons. *J Clim* 18:4150–4167
- Belkin IM (2009) Rapid warming of Large Marine Ecosystems. *Prog Oceanogr* 81:207–213
- Belkin IM, Lee MA (2014) Long-term variability of sea surface temperature in Taiwan Strait. *Clim Change* 124:821–834
- Boggs S, Wang WC, Lewis FS, Chen JC (1979) Sediment properties and water characteristics of the Taiwan shelf and slope. *Acta Oceanogr Taiwan* 10:10–49
- Chang CP, Lau KM (1982) SHORT-TERM PLANETARY-SCALE INTERACTIONS OVER THE TROPICS AND MID-LATITUDES DURING NORTHERN WINTER.1. CONTRASTS BETWEEN ACTIVE AND INACTIVE PERIODS. *Mon Weather Rev* 110:933–946
- Chang Y, Lee KT, Lee MA, Lan KW (2009) Satellite Observation on the Exceptional Intrusion of Cold Water in the Taiwan Strait. *Terr Atmos Ocean Sci* 20:661–669
- Chen HW, Coauthors (2016) Temporal variations of volume transport through the Taiwan Strait, as identified by three-year measurements. *Cont Shelf Res* 114:41–53
- Cheng YH, Chang MH (2018) Exceptionally cold water days in the southern Taiwan Strait: their predictability and relation to La Nina. *Nat Hazards Earth Syst Sci* 18:1999–2010
- Chhak KC, Di Lorenzo E, Schneider N, Cummins PF (2009) Forcing of Low-Frequency Ocean Variability in the Northeast Pacific. *J Clim* 22:1255–1276
- Di Lorenzo E, Coauthors (2010) Central Pacific El Nino and decadal climate change in the North Pacific Ocean. *Nat Geosci* 3:762–765

- Di Lorenzo E, and Coauthors (2008) North Pacific Gyre Oscillation links ocean climate and ecosystem change. *Geophys Res Lett* 35:6
- Ding Y, Krishnamurti TN (1987) HEAT-BUDGET OF THE SIBERIAN HIGH AND THE WINTER MONSOON. *Mon Weather Rev* 115:2428–2449
- Ehteram M, Mousavi SF, Karami H, Farzin S, Singh VP, Chau KW, El-Shafie A (2018) Reservoir operation based on evolutionary algorithms and multi-criteria decision-making under climate change and uncertainty. *J Hydroinform* 20:332–355
- Gershunov A, Barnett TP (1998) Interdecadal modulation of ENSO teleconnections. *Bull Amer Meteorol Soc* 79:2715–2725
- Gong DY, Wang SW, Zhu JH (2001) East Asian winter monsoon and Arctic Oscillation. *Geophys Res Lett* 28:2073–2076
- Guan BX, Fang GH (2006) Winter counter-wind currents off the southeastern China coast: A review. *J Oceanogr* 62:1–24
- He SP, Wang HJ (2013) Oscillating Relationship between the East Asian Winter Monsoon and ENSO. *J Clim* 26:9819–9838
- Hong HS, Chai F, Zhang CY, Huang BQ, Jiang YW, Hu JY (2011) An overview of physical and biogeochemical processes and ecosystem dynamics in the Taiwan Strait. *Cont Shelf Res* 31:S3–S12
- Hook BA, Halfar J, Gedalof Z, Bollmann J, Schulze DJ (2015) Stable isotope paleoclimatology of the earliest Eocene using kimberlite-hosted mummified wood from the Canadian Subarctic. *Biogeosciences* 12:5899–5914
- Hsieh HJ, Hsien YL, Jeng MS, Tsai WS, Su WC, Chen CA (2008) Tropical fishes killed by the cold. *Coral Reefs* 27:599–599
- Hu JY, Kawamura H, Li CY, Hong HS, Jiang YW (2010) Review on Current and Seawater Volume Transport through the Taiwan Strait. *J Oceanogr* 66:591–610
- Huang RH, Zhou LT, Chen W (2003) The progresses of recent studies on the variabilities of the East Asian monsoon and their causes. *Adv Atmos Sci* 20:55–69
- Huang RH, Chen JL, Huang G (2007) Characteristic's and variations of the East Asian monsoon system and its impacts on climate disasters in China. *Adv Atmos Sci* 24:993–1023
- Huang WY, Chen RY, Yang ZF, Wang B, Ma WQ (2017) Exploring the combined effects of the Arctic Oscillation and ENSO on the wintertime climate over East Asia using self-organizing maps. *J Geophys Res -Atmos* 122:9107–9129
- Jan S, Sheu DD, Kuo HM (2006) Water mass and throughflow transport variability in the Taiwan Strait. *J Geophys Res -Oceans* 111:15
- Jan S, Wang J, Chern CS, Chao SY (2002) Seasonal variation of the circulation in the Taiwan Strait. *J Mar Syst* 35:249–268
- Jiang H, Jin QH, Wang H, Huang RX (2013) Indices of strength and location for the North Pacific Subtropical and Subpolar Gyres. *Acta Oceanol Sin* 32:22–30
- Joh Y, Di Lorenzo E (2017) Increasing Coupling Between NPGO and PDO Leads to Prolonged Marine Heatwaves in the Northeast Pacific. *Geophys Res Lett* 44:11663–11671
- Kim JW, Yeh SW, Chang EC (2014) Combined effect of El Niño-Southern Oscillation and Pacific Decadal Oscillation on the East Asian winter monsoon. *Clim Dyn* 42:957–971
- Kim JW, An SI, Jun SY, Park HJ, Yeh SW (2017) ENSO and East Asian winter monsoon relationship modulation associated with the anomalous northwest Pacific anticyclone. *Clim Dyn* 49:1157–1179
- Lee MA, Yang YC, Shen YL, Chang Y, Tsai WS, Lan KW, Kuo YC (2014) Effects of an Unusual Cold-Water Intrusion in 2008 on the Catch of Coastal Fishing Methods around Penghu Islands, Taiwan. *Terr Atmos Ocean Sci* 25:107–120
- Levine AFZ, McPhaden MJ, Frierson DMW (2017) The impact of the AMO on multidecadal ENSO variability. *Geophys Res Lett* 44:3877–3886
- Liao EH, Yan XH, Jiang YW, Kidwell AN (2019) New findings on the route of heat transport between the Indo-Pacific and Southern Ocean. *Clim Dyn* 52:5145–5151
- Liao EH, Jiang YW, Li L, Hong HS, Yan XH (2013) The cause of the 2008 cold disaster in the Taiwan Strait. *Ocean Model* 62:1–10.
- Liao EH, Lu WF, Yan XH, Jiang YW, Kidwell A (2015) The coastal ocean response to the global warming acceleration and hiatus. *Sci Rep* 5:10
- Liao EH, Oey LY, Yan XH, Li L, Jiang YW (2018) The Deflection of the China Coastal Current over the Taiwan Bank in Winter. *J Phys Oceanogr* 48:1433–1450
- Lima FP, Wethey DS (2012) Three decades of high-resolution coastal sea surface temperatures reveal more than warming. *Nat Commun* 3:13
- Liu ZY, Lorenzo ED (2018) Mechanisms and Predictability of Pacific Decadal Variability. *Curr Clim Chang Rep* 4:128–144
- Ma TJ, Chen W (2021) : Climate variability of the East Asian winter monsoon and associated extratropical-tropical interaction: a review. *Ann. N.Y. Acad. Sci.*, 19
- Mantua NJ, Hare SR, Zhang Y, Wallace JM, Francis RC (1997) A Pacific interdecadal climate oscillation with impacts on salmon production. *Bull Amer Meteorol Soc* 78:1069–1079
- Oey LY, Wang J, Lee MA (2018) Fish Catch Is Related to the Fluctuations of a Western Boundary Current. *J Phys Oceanogr* 48:705–721
- Oey LY, Chang MC, Chang YL, Lin YC, Xu FH (2013) Decadal warming of coastal China Seas and coupling with winter monsoon and currents. *Geophys Res Lett* 40:6288–6292
- Oey LY, Chang YL, Lin YC, Chang MC, Varlamov S, Miyazawa Y (2014) Cross Flows in the Taiwan Strait in Winter\*. *J Phys Oceanogr* 44:801–817
- Pan AJ, Wan XF, Guo XG, Jing CS (2013) Responses of the Zhe-Min coastal current adjacent to Pingtan Island to the wintertime monsoon relaxation in 2006 and its mechanism. *Sci China-Earth Sci* 56:386–396
- Parkinson CL, Vinnikov KY, Cavalieri DJ (2006) Evaluation of the simulation of the annual cycle of Arctic and Antarctic sea ice coverages by 11 major global climate models (vol 111, art no C07012, 2006). *J Geophys Res -Oceans* 111:6
- Rayner NA, Coauthors (2003) Global analyses of sea surface temperature, sea ice, and night marine air temperature since the late nineteenth century. *J Geophys Res -Atmos* 108:37
- Rayner NA, Coauthors (2006) Improved analyses of changes and uncertainties in sea surface temperature measured in situ since the mid-nineteenth century: The HadSST2 dataset. *J Clim* 19:446–469
- Reynolds RW, Chelton DB (2010) Comparisons of Daily Sea Surface Temperature Analyses for 2007–08. *J Clim* 23:3545–3562
- Rogers JC (1981) The North Pacific Oscillation. *J Climatol* 1:39–57
- Schlesinger ME, Ramankutty N (1994) An oscillation in the global climate system of period 65–70 years. *Nature* 367:723–726
- Sharafati A, Pezeshki E (2020) A strategy to assess the uncertainty of a climate change impact on extreme hydrological events in the semi-arid Dehbar catchment in Iran. *Theor Appl Climatol* 139:389–402
- Torrence C, Compo GP (1998) A practical guide to wavelet analysis. *Bull Amer Meteorol Soc* 79:61–78
- Wallace JM, Gutzler DS (1981) Teleconnections in the geopotential height field during the northern hemisphere winter. *Mon Weather Rev* 109:784–812
- Wang B, Wu RG, Fu XH (2000) Pacific-East Asian teleconnection: how does ENSO affect East Asian climate? *J Clim* 13:1517–1536
- Wang B, Wu ZW, Chang CP, Liu J, Li JP, Zhou TJ (2010) Another Look at Interannual-to-Interdecadal Variations of the East Asian Winter Monsoon: The Northern and Southern Temperature Modes. *J Clim* 23:1495–1512

- Wang CZ, Picaut J (2002) : Understanding ENSO physics - A review. *Conference on Ocean-Atmosphere Interaction and Climate Variability*, San Francisco, CA, Amer Geophysical Union, 21–48
- Wang J, Ikeda M (2000) Arctic oscillation and Arctic sea-ice oscillation. *Geophys Res Lett* 27:1287–1290
- Wang J, Oey LY (2014) Inter-annual and decadal fluctuations of the Kuroshio in East China Sea and connection with surface fluxes of momentum and heat. *Geophys Res Lett* 41:8538–8546
- Wang J, Hong H, Jiang Y, Chai F, Yan X-H (2013) Summer nitrogenous nutrient transport and its fate in the Taiwan Strait: A coupled physical-biological modeling approach. *J Geophys Res -Oceans* 118:4184–4200
- Wang L, Chen W, Huang RH (2008) Interdecadal modulation of PDO on the impact of ENSO on the east Asian winter monsoon. *Geophys Res Lett* 35:4
- Webster PJ, Magana VO, Palmer TN, Shukla J, Tomas RA, Yanai M, Yasunari T (1998) Monsoons: Processes, predictability, and the prospects for prediction. *J Geophys Res -Oceans* 103:14451–14510
- Wu BY, Zhang RH, D'Arrigo R (2006) Distinct modes of the East Asian winter monsoon. *Mon Weather Rev* 134:2165–2179
- Wu ZW, Li JP, Wang B, Liu XH (2009) Can the Southern Hemisphere annular mode affect China winter monsoon? *J Geophys Res -Atmos* 114:11
- Xu ZL, Gao Q, Kang W, Zhou J (2013) Regional warming and decline in abundance of *Euchaeta Plana* (Copepoda, Calanoida) in the nearshore waters of the east China Sea. *J Crustac Biol* 33:323–331
- Yang JY (2007) An oceanic current against the wind: How does Taiwan island steer warm water into the East China Sea? *J Phys Oceanogr* 37:2563–2569
- Zhang RH, Sumi A, Kimoto M (1996) Impact of El Nino on the East Asian monsoon: A diagnostic study of the '86/87 and '91/92 events. *J Meteorol Soc Jpn* 74:49–62
- Zhang RH, Min QY, Su JZ (2017) Impact of El Nino on atmospheric circulations over East Asia and rainfall in China: Role of the anomalous western North Pacific anticyclone. *Sci China-Earth Sci* 60:1124–1132
- Zhang Y, Sperber KR, Boyle JS (1997) Climatology and interannual variation of the East Asian winter monsoon: Results from the 1979-95 NCEP/NCAR reanalysis. *Mon Weather Rev* 125:2605–2619
- Zhao CP, Huang YH, Li ZH, Chen MX (2018) Drought Monitoring of Southwestern China Using Insufficient GRACE Data for the Long-Term Mean Reference Frame under Global Change. *J Clim* 31:6897–6911
- Zhao ZH, Lin JW, Fu J, Jiang YW (2020) Cold water anomalies in the middle layer of the northern Taiwan Strait in spring-a numerical approach. *Ocean Dyn* 70:1571–1585

**Publisher's Note** Springer Nature remains neutral with regard to jurisdictional claims in published maps and institutional affiliations.

## Terms and Conditions

Springer Nature journal content, brought to you courtesy of Springer Nature Customer Service Center GmbH (“Springer Nature”).

Springer Nature supports a reasonable amount of sharing of research papers by authors, subscribers and authorised users (“Users”), for small-scale personal, non-commercial use provided that all copyright, trade and service marks and other proprietary notices are maintained. By accessing, sharing, receiving or otherwise using the Springer Nature journal content you agree to these terms of use (“Terms”). For these purposes, Springer Nature considers academic use (by researchers and students) to be non-commercial.

These Terms are supplementary and will apply in addition to any applicable website terms and conditions, a relevant site licence or a personal subscription. These Terms will prevail over any conflict or ambiguity with regards to the relevant terms, a site licence or a personal subscription (to the extent of the conflict or ambiguity only). For Creative Commons-licensed articles, the terms of the Creative Commons license used will apply.

We collect and use personal data to provide access to the Springer Nature journal content. We may also use these personal data internally within ResearchGate and Springer Nature and as agreed share it, in an anonymised way, for purposes of tracking, analysis and reporting. We will not otherwise disclose your personal data outside the ResearchGate or the Springer Nature group of companies unless we have your permission as detailed in the Privacy Policy.

While Users may use the Springer Nature journal content for small scale, personal non-commercial use, it is important to note that Users may not:

1. use such content for the purpose of providing other users with access on a regular or large scale basis or as a means to circumvent access control;
2. use such content where to do so would be considered a criminal or statutory offence in any jurisdiction, or gives rise to civil liability, or is otherwise unlawful;
3. falsely or misleadingly imply or suggest endorsement, approval, sponsorship, or association unless explicitly agreed to by Springer Nature in writing;
4. use bots or other automated methods to access the content or redirect messages
5. override any security feature or exclusionary protocol; or
6. share the content in order to create substitute for Springer Nature products or services or a systematic database of Springer Nature journal content.

In line with the restriction against commercial use, Springer Nature does not permit the creation of a product or service that creates revenue, royalties, rent or income from our content or its inclusion as part of a paid for service or for other commercial gain. Springer Nature journal content cannot be used for inter-library loans and librarians may not upload Springer Nature journal content on a large scale into their, or any other, institutional repository.

These terms of use are reviewed regularly and may be amended at any time. Springer Nature is not obligated to publish any information or content on this website and may remove it or features or functionality at our sole discretion, at any time with or without notice. Springer Nature may revoke this licence to you at any time and remove access to any copies of the Springer Nature journal content which have been saved.

To the fullest extent permitted by law, Springer Nature makes no warranties, representations or guarantees to Users, either express or implied with respect to the Springer nature journal content and all parties disclaim and waive any implied warranties or warranties imposed by law, including merchantability or fitness for any particular purpose.

Please note that these rights do not automatically extend to content, data or other material published by Springer Nature that may be licensed from third parties.

If you would like to use or distribute our Springer Nature journal content to a wider audience or on a regular basis or in any other manner not expressly permitted by these Terms, please contact Springer Nature at

[onlineservice@springernature.com](mailto:onlineservice@springernature.com)